Live cell monitoring of double strand breaks in *S. cerevisiae*

David P. Waterman, Cheng-Sheng Lee, Michael Tsabar, Felix Zhou, Vinay V. Eapen, Allison Mazzella and James E. Haber*

Rosenstiel Basic Medical Science Center and the Department of Biology, Brandeis University, Waltham, MA, 02454

Corresponding author
Email: haber@brandeis.edu

Abstract

We have used two different live-cell fluorescent protein markers to monitor the formation and localization of double-strand breaks (DSBs) in budding yeast. Using GFP derivatives of the Rad51 recombination protein or the Ddc2 checkpoint protein, we find that cells with three site-specific DSBs, on different chromosomes, usually display 2 or 3 foci that coalesce and dissociate. Rad51-GFP, by itself, is unable to repair DSBs by homologous recombination in mitotic cells, but is able to form foci and allow repair when heterozygous with a wild type Rad51 protein. The kinetics of disappearance of Rad51-GFP foci parallels the completion of DSB repair. However, in meiosis, Rad51-GFP is proficient when homozygous. Using Ddc2-GFP, we conclude that co-localization of foci following 3 DSBs does not represent formation of a homologous recombination "repair center," as the same distribution of Ddc2-GFP foci was found in the presence or absence of the Rad52 protein. The maintenance of separate DSB foci and much of their dynamics depend on functional microtubules, as addition of nocodazole resulted in a greater population of cells displaying a single focus.

Author Summary

Double strand breaks (DSBs) pose the greatest threat to the fidelity of an organism's genome. While much work has been done on the mechanisms of DSB repair, the arrangement and interaction of multiple DSBs within a single cell remain unclear. Using two live-cell fluorescent DSB markers, we show that cells with 3 site-specific DSBs usually form 2 or 3 foci what can coalesce into fewer foci but also dissociate. The aggregation of DSBs into a single focus does not depend on the Rad52 recombination protein, suggesting that there is no "repair center" for homologous recombination. DSB foci are highly dynamic and their dynamic nature is dependent on microtubules.

Introduction

The process of repairing chromosomal double-strand breaks by Rad51- and Rad52-mediated homologous recombination in budding yeast has been defined by a combination of in vitro analysis of purified recombination proteins (1-3) and from

"in vivo biochemistry" analyses of the kinetics of repair of site-specific DSBs (4). Cleaved DNA ends are attacked by several 5' to 3' exonucleases to produce long 3'-ended single-strand DNA (ssDNA) tails, which are initially coated by the single-strand binding complex, RPA (5, 6). RPA is displaced by Rad51 recombinase through the action of mediator proteins, including Rad52, creating a nucleoprotein filament composed primarily of Rad51 but also its paralogs, the Rad55-Rad57 heterodimer (7-9). The Rad51 filament engages in a genome-wide search for a homologous sequence that could be on a sister chromatid, a homologous chromosome or at an ectopic location. Once the donor sequence is encountered, Rad51 catalyzes strand exchange to form a D-loop intermediate, the initial step in repair. The 3' end of the invading strand then acts as a primer to initiate new DNA synthesis that leads to repair of the DSB via several pathways including gene conversion via synthesis-dependent strand annealing or a double Holliday junction pathway. A combination of Southern blot, PCR and chromatin immunoprecipitation (ChIP) experiments have shown that DSB repair proceeds by a series of kinetically slow steps, taking more than an hour to complete (reviewed in (4)).

In haploid cells, successful recombination with an ectopic donor sequence is strongly dictated by the contact probability of sequences within different chromosomes (10, 11). When the ends of the DSB fail to encounter a donor, or in the case where there is no donor, an unrepaired break eventually enters a different pathway, where it associates with the nuclear envelope through its association with the nuclear envelope protein Mps3 (12). Localization to the envelope may alter further end-resection and may facilitate joining of DSB ends by nonhomologous end-joining (13).

One approach to the study of DSB repair in budding yeast has been the use of live-cell microscopy to monitor the behavior of different fluorescently tagged repair-associated proteins. The most thoroughly studied is Rad52, the key mediator for the assembly of the Rad51 filament, but which is also critical in later strand-annealing steps(14). Strikingly when there are multiple DSBs, created by ionizing radiation or

by site-specific endonucleases, there often appears to be a single fluorescent Rad52 focus. This observation has led to the idea that there could be a "repair center" where recombination proteins might accumulate to facilitate DSB repair (15). However, immunofluorescent staining of spread nuclei with multiple DSBs found that the number of foci directly correlated with the number of DSBs (16)

A limitation in extending these studies has been the absence of other live-cell markers to follow repair. To this end, we constructed and characterized a Rad51-GFP fusion protein. Previously, a Rad51-GFP fusion was characterized in *Arabidopsis*, where it proved to be defective in mitotic DSB repair, but competent in meiosis (17). This phenotype resembles the "site II" mutation of *Saccharomyces cerevisiae* Rad51, which can bind ssDNA but is unable to bind dsDNA and thus fails to complete strand invasion and DSB repair in mitotic cells (18, 19). Similar results were obtained using a human isoform of Rad51-GFP *in vitro* (20). In fission yeast, scRad51's homolog Rhp51 when fused with CFP proved to be UV sensitive and incapable of carrying our repair on its own, but this defect was complimented by expression of wild type Rhp51 (21). Here we show that yeast Rad51-GFP binds to site-specific DSBs in mitotic cells but cannot catalyze homologous recombination when it is the only allele present; however, it is not dominant-negative - as is a similar construct in *Arabidopsis* (17). Consequently, Rad51-GFP can be used to follow GFP-labeled filaments that are engaged in functional recombination. In meiosis, budding yeast Rad51 acts as an auxiliary factor with the Rad51 homolog, Dmc1, and the site II mutant is competent for meiotic recombination (18). As with the *Arabidopsis* construct, yeast Rad51-GFP is competent for meiosis. Thus, we have developed a live-cell reporter for Rad51 in response to DSBs in both mitotic and meiotic cells where recombination can be induced synchronously.

Using either Rad51-GFP or a GFP fusion of the DNA damage checkpoint protein Ddc2, yeast's homolog of the ATRIP protein that has been previously shown to bind near a DSB and to recruit $Mec1^{ATR}$ kinase (22, 23), we show that cells which have multiple site-specific DSBs form multiple, highly dynamic GFP foci that coalesce and

separate. In the majority of these cases, there are also multiple Rad52 foci, although some limitation in Rad52-RFP expression or a propensity for self-aggregation appears to restrict the number of Rad52-RFP foci even when there are distinct GFP foci. These results suggest that multiple DSBs do not generally form a Rad52-dependent repair center.

Results

Rad51-GFP forms a DNA damage-dependent focus

An ideal tool for monitoring DSB formation and repair would be a fluorescent protein that performs a central role in homologous recombination. We created a Rad51-GFP fusion construct utilizing a -SSGSSG- linker, which we have previously used to increase the functionality of other fusion proteins (24). We integrated this construct at the C-terminus of the genomic copy of *RAD51* in the donorless, galactose inducible HO-inducible strain JKM179 in which a single irreparable DSB is induced upon addition of galactose (25). More than 70% of cells displayed a single GFP focus within 3 h after inducing HO expression, increasing to >90% by 5 h (Figure 1D and S1A). Rad51-GFP foci were absent in *rad52*Δ cells or in cells that lack an HO cleavage site (Figures 1 and S1). When Rad51-GFP was coexpressed with Rad52-RFP, green and red foci colocalized (Figure 1F, S1D).

Rad51 has been shown to increase in abundance after DNA damage (26, 27). Such an increase is evident comparing the total nuclear intensity of Rad51-GFP in cells with a DSB (with or without Rad52) compared to cells lacking the HO cleavage site (Figure 1E).

To test directly if Rad51-GFP was bound to the DNA around the DSB, we performed chromatin immunoprecipitation using an antibody recognizing Rad51 to assay Rad51-GFP accumulation 5 kb from the DSB induced in the *MAT*α locus in a derivative of strain JKM179, lacking donor sequences, as described previously (28). As shown in Figure 1G, Rad51-GFP binding 5 kb from the unrepaired DSB end

increased steadily over 6 h. Rad51-GFP binding appears similar in its kinetics to wild type Rad51, as measured previously (19, 28). Therefore, Rad51-GFP effectively binds to resected DNA around a DSB and thus shows promise for further live cell studies.

Rad51-GFP cannot repair DSBs by homologous recombination in mitotic cells, but it is not dominant negative.

Next, we sought to determine whether Rad51-GFP was functional with regard to the DNA damage checkpoint and to DSB repair. Cells that suffer an irreparable DSB arrest for 9-12 h through activation of the DNA damage checkpoint. After about 12 h, and without repairing the DSB, yeast cells switch off the checkpoint and proceed through mitosis in a process called adaptation (25, 29, 30). Adaptation requires Rad51, but not Rad52; in *rad51*Δ most cells permanently arrest prior to mitosis after a DSB (31). However, Rad51-GFP cells are capable of adapting similar to wild type (Figure 2A).

In the assays described thus far, the DSBs were irreparable by HR because of the lack of a donor template. To investigate the ability of Rad51-GFP to participate in HR, we turned to strain YJK17, in which there is a DSB at *MAT*α on Chr3 and a single ectopic *MAT***a**-inc donor sequence on Chr5 (32). An HO break is repaired in roughly 80% of cells over the course of 6-9 h. YJK17 carrying Rad51-GFP failed to repair the DSB (Fig. 2B). Given the multimeric nature of the Rad51 filament and that many Rad51 mutations are dominant-negative (33 , 34) we asked if Rad51-GFP is dominant negative. We found that HO-induced DSB repair in YJK17 was repair-proficient after introducing wild type Rad51 on a centromeric plasmid, expressed from the its own promoter (Figure 2B). The kinetics of repair, monitored by qPCR, were very similar for Rad51-GFP complemented by *RAD51* compared to wild type (Figure 2D). In parallel with repair, the percent of cells displaying a GFP focus decreased from 80% at 4 h to ~50% by 7 h and fewer than 30% by 9 h, whereas

without the complementing Rad51, foci persisted (Figure 2C). This decreased correlated with the timing of repair as monitored by qPCR (Figure 2C).

Further evidence that Rad51-GFP is not dominant-negative was found by monitoring cells exposed to 0.002% MMS, which was lethal to Rad51-GFP cells but not to wild type (Figure 2E). The sensitivity of the Rad51-GFP strain was rescued by providing wild type *RAD51*, expressed from its own promoter, on a centromere-containing plasmid. These data suggest that Rad51-GFP is capable of binding DNA even in the presence of wild type Rad51 and the GFP fusion's loss of function can be complimented by expression of wild type Rad51.

Rad51-GFP is competent in meiosis

Arabidopsis Rad51-GFP proved to be meiosis-competent even though it blocked mitotic recombination (17). As noted above, this phenotype resembles a Rad51 "site II" mutation in budding yeast (18). In meiosis, the critical functions of strand exchange depend on Rad51's homolog, Dmc1, with Rad51 acting in an apparently allosteric fashion. We found that Rad51-GFP is meiosis-proficient. Diploids homozygous or heterozygous for Rad51-GFP produced the same percentage of as wild type. (Figure 3A). After tetrad dissection, spores resulting from diploids homozygous for Rad51-GFP exhibited a 40% reduction in spore viability, but nevertheless 60% of spores were viable (Figure 3B). Thus, *S. cerevisiae* Rad51-GFP strongly resembles a site II mutation (18).

Multiple DSBs form discrete Rad51-GFP foci

We extended our analysis to monitor the appearance of multiple DSBs, to determine whether multiple DSBs would appear as a single Rad51-GFP focus or as distinct Rad51-GFP foci. We inserted Rad51-GFP into strain YCSL004 carrying 3 HO cleavage sites, each on a different chromosome, as well as Rad52-RFP, and counted the number of foci 3 h after *GAL::HO* induction. We observed an average of 2 Rad51-GFP foci (Figures 4A, B, S2A). This distribution was unchanged in *lig4*Δ cells, in which repair by end-joining is blocked (35-37)(Figure S2B).

In wild type cells, we noticed several instances of cells displaying a single Rad52-RFP focus but multiple Rad51-GFP foci (Figures 4Aiii and B). In these cells, the single Rad52-RFP focus was typically large and always colocalized with a single Rad51-GFP focus. Therefore, monitoring the number and locations of DSBs via Rad52 may not serve as a realistic reflection of the actual DSB state.

We also examined Rad51-GFP foci in strains with 6 HO cleavage sites (38). We observed a range of the number of foci per cell, averaging 3.2 foci, 6 h after HO induction (Figures 4C, D, and S2C).

Live cell detection of DSBs with Ddc2-GFP

In strains with multiple DSBs, only a small proportion display a single Rad51-GFP focus, raising the question whether DSBs are usually recruited into a repair center. However, whether the distribution of foci depends on Rad52 is impossible to test using Rad51-GFP, as Rad51's recruitment is completely dependent on Rad52 (28, 39). To directly ask whether Rad52 recruits multiple DSBs to the same location in the nucleus, we monitored DSB dynamics using a live cell marker that is independent of Rad52.

One such candidate is the DNA damage checkpoint protein Ddc2. Ddc2 localizes to a broken DNA end, either directly or by binding to RPA (22, 23, 40) and previous studies have shown strong localization of Ddc2-GFP at DSB sites (41-43). We carried out an analysis similar to that described above for Rad51-GFP, using a derivative of strain YSCL004 with 3 HO-induced DSBs but carrying an insertion of GFP at the C-terminus of the chromosomal copy of Ddc2 (strain VE290). Again, we observed cells with 1, 2, or 3 foci with an average of 2 foci per cell (Figures 5A, B, and S3A). We repeated this analysis in a *rad52*Δ derivative and found no difference in the distribution of Ddc2-GFP foci (Figures 5B and S3B). Hence, Ddc2 foci are not dependent on Rad52. However, in *rad52*Δ, we noticed a small percentage of cells

that had more than 3 foci (Figure 5B, S3B, Movies S1-S3). In 5.4% of *rad52*Δ cells, 4 and sometimes 5 foci were evident (Figure 5B), suggesting that Rad52 might be partially responsible for holding together the ends of DSBs.

Even in the absence of Rad52, we observed ~25% of cells displaying a single focus. It is possible that in single-focus cells, HO had not efficiently cut all three sites. To address this possibility, we took advantage of the high signal specificity and low nuclear background signal in cells expressing Ddc2-GFP to determine the fluorescent signal intensity of individual foci. It is evident that the intensity of the single focus was much greater than the average intensities of each focus in cells displaying 2 foci or 3 foci. Indeed, the signal intensity of 1 focus is equal to the sum of the signal intensities of 3 foci (Figure 5C). Thus, cells with a single focus apparently have 3 DSBs that are indeed co-localized. These intensities were unchanged in *rad52*Δ (Figure 5C).

DSB foci are dynamic

Chromosomal mobility and chromatin persistence length are radically altered after the induction of a DSB (44-46). We examined the stability of foci with 3 DSBs DSB by observing cells using over a ten minute period 3 h after HO induction, using spinning disk confocal microscopy. In 85% of cases, the number and general localization of foci in a given cell remained constant over 10 min (Movies S7-S10). However, in 15% of cells, we observed changes in the number of Ddc2-GFP foci. We found instances when the number of foci diminished, from three to two or from two to one, as well as a single focus splitting into two or three foci (Figure 5E, Movies S11 – S17). This behavior was unchanged in *rad5*2Δ, with the exception of a few cells with >3 foci described above. We conclude that DSBs are dynamic and that Rad52 is not the mediator of a DSB repair center.

Microtubules control DSB dynamics

Due to the dynamic nature of multiple DSBs, we sought to determine the molecular mechanism behind this motion. The spindle pole, microtubules, and the kinetochore have all been implicated in governing chromatin mobility in response to DNA damage (47, 48). Furthermore, DSBs have been shown to colocalize with spindle pole bodies preferentially loaded with the SUN protein Mps3 (12, 49). However, in our 3-DSB system expressing Ddc2-GFP and Mps3-mCherry, we find only 28% of cells exhibit Ddc2/Mps3 colocalization (Figure 6A). To test whether the action of microtubules was required for DSB dynamics in our system, we induced HO for 3 h in cells suffering 3 DSBs and expressing Ddc2-GFP. After 2 h, we added nocodazole for 1 h then monitored foci dynamics by live cell confocal microscopy (Figure 6B). The distribution of foci per cell was drastically shifted towards many more single focus cells (Figure 6C). Thus, DSB dynamics are driven by microtubules and in the absence of microtubules multiple DSBs colocalize.

Discussion

DSB repair must be coordinated in space and time in order to faithfully repair lesions to the genome. The role of many proteins involved in DSB repair has been elucidated through in vitro and in vivo biochemistry, but the lack of suitable live cells markers has provided a barrier to studying DSB repair in real-time. Here, we report DSB dynamics in single- and multiple-break conditions using two different fluorescently tagged proteins that carry out different functions in response to DNA damage; the recombinase Rad51-GFP and the checkpoint-related protein Ddc2-GFP. In both cases, multiple DSBs resulted in multiple fluorescent foci.

Using Rad51-GFP or Ddc2-GFP in our 3 DSB system, the majority of cells exhibit two or three foci. Rad51-GFP foci often colocalize with Rad52-RFP, but we see many instances with more GFP foci than RFP foci. Previous studies have looked specifically at the role of Rad52 in organizing a “repair center” yeast (15, 50). Our data suggests that monitoring Rad52 focus formation may underestimate the number of DSBs throughout the nucleus. This difference may in part reflect the temporal recruitment of DSB repair proteins to the site of DSBs such that the

304 continued presence of Rad52 at a DSB may not be necessary once a Rad51 filament
305 has been established.
306
307 While our Rad51-GFP construct is not able, by itself, to repair DSBs by homologous
308 recombination, it is not dominant negative and supports recombination in meiosis.
309 Biochemical work on a human isoform of Rad51 fused to GFP determined that the
310 fluorescent tag prevented Rad51 from engaging in the pairing of homologous
311 sequences by inhibiting Rad51's secondary DNA binding (20). We envision the
312 same to be true of our Rad51-GFP construct because our ChIP experiments and
313 microscopy suggest that Rad51-GFP can efficiently bind to ssDNA and form a
314 filament, its first step in homologous recombination. However, when Rad51-GFP is
315 the sole copy of Rad51 in cells, DSB repair by homologous recombination is
316 incomplete, presumably at the strand exchange step.
317
318 Rad51-GFP's defect in ectopic gene conversion is suppressed by addition of a single
319 second copy of wild type Rad51 expressed from its endogenous promoter. Likewise,
320 the MMS sensitivity conferred by Rad51-GFP was also rescued by expression of wild
321 type Rad51. However, it is not that wild type Rad51 simply excludes Rad51-GFP
322 from binding ssDNA, since Rad51-GFP readily forms a focus in the presence of wild
323 type Rad51. This is similar to a similar construct reported in fission yeast (21).
324 Together with previous reports, data suggest either that a functional Rad51 filament
325 does not require every Rad51 molecule to be functional or that subunit-subunit
326 interactions between wild type and GFP-tagged Rad51 corrects the defect. The
327 exact stoichiometry for a functional filament cannot be determined from these
328 experiments, but from previous work done by our lab (51) we speculate that there
329 need to be at least two to three functional Rad51 molecules in tandem to facilitate
330 minimal Rad51-mediated strand exchange.
331
332 To directly test whether Rad52 recruits multiple DSBs into a common locus, we
333 used Ddc2-GFP, which forms foci independent of Rad52. In our 3-DSB strain, we see
334 an average of 2 Ddc2-GFP foci per cell, but still about 25% of cells display a single

335 focus, as with Rad51-GFP. However, this distribution remains unchanged in a
336 *rad52*Δ derivative. Therefore, we conclude that Rad52 is not required for
337 organizing multiple DSBs into one specific nuclear location. However, Rad52
338 appears to be partially responsible for tethering the ends of the DSB together, as we
339 see a small but significant population of cells with greater than 3 Ddc2-GFP foci in
340 *rad52*Δ. Both the Ku complex and Mre11 have been implicated in DBS end tethering
341 previously (52, 53), but this study is the first to suggest that Rad52 is also a key
342 player in end tethering.
343
344 That DSB foci are dynamic also supports our model that DSBs do not generally form
345 a repair center. Increased chromatin motion in response to a DSB is believed to aid
346 in DNA repair through facilitating in homology search throughout the genome (44-
347 46) but the precise mechanism for this motion is relatively unclear. A recent study
348 from the Durocher lab demonstrated that the DNA damage checkpoint kinase
349 cascade targets the kinetochore-associated protein Cep3 and this phosphorylation
350 increases chromatin movement through activation of the spindle assembly
351 checkpoint (47). Similarly, increased chromatin movement in response to a single
352 DSB has been shown to be microtubule dependent (48). In our system, functional
353 microtubules promote DSB dynamics; in their absence, DSBs tend to coalesce.
354 However, given that the foci distribution in three HO break cells are not altered in
355 *rad52*Δ, the exact mechanism behind this coalescence remains to be determined.
356
357 **Materials and Methods**
358
359 **Strain and Plasmid Construction:**
360 Standard yeast genome manipulation procedures were used for all strain
361 constructions (54). Linear DNA and plasmids were introduced by the standard
362 lithium acetate transformation procedure (55). To C-terminally tag Rad51 and Ddc2
363 with GFP, PCR primers were used to amplify the GFP fragment from pFA6a-
364 GFP(S65T) and the *TRP1* or KAN selectable marker in the Longtine collection (56)

and introduced to the appropriate parent strain by lithium acetate transformation. Strain genotypes are listed in Table S1. Primer sequences are listed in Table S2.

Growth Conditions:

To visualize the chromosomally integrated fluorescent tags (Rad51-GFP and Ddc2-GFP) after DNA damage, cells from a single colony were grown overnight in 5ml YEP + 4% lactic acid (YPLac). Cells were diluted to OD600 = 0.2 and grown for 4 h in 5 ml of fresh YPLac before addition of galactose to a final concentration of 2% to induce *GAL::HO* expression. For experiments that visualized Rad52-RFP, the same growth procedure except that cells were grown in SD-leucine media supplemented with 2% raffinose.

Plating Assays and Viability

The efficiency of DSB repair by homologous recombination was determined as described previously for strain YJK17 (32). Briefly, cells of the appropriate strain were selected from a single colony on YPD plates and grown overnight in 5 ml of YPLac. Cells were diluted to OD600 = 0.2 and allowed to grow until OD600 = 0.5 – 1.0. Approximately 100 cells from each culture were then plated on YPGal (2% v/v) and YPD in triplicate and incubated at 30 °C. Viability was calculated by dividing the number of colonies on YPGal by the number of colonies on YPD.

Adaptation assays in strain JKM179 were performed as previously described (24). Briefly, cells were grown in YPLac or SD- media supplemented with 2% raffinose overnight then individual unbudded (G1) cells were plated on YPGal and observed microscopically for 24 h to determine the percent that were arrested in the G2/M stage of the cell cycle.

Viability on MMS media was determined by as described by (57) . Cells of the appropriate strain were selected from a single colony on YPD plates and grown overnight in 5 ml of selective media to near saturation. The following day, cultures were diluted to OD600 = 0.2 and left to grow at 30 °C for 3-5 doublings. Cells were

396 then diluted in 200 µl sterile water to OD600 = 0.2 in a 96-well plate and
397 subsequently 10-fold serially diluted six times. Cell dilutions were then plated on
398 YPD, -leu, and -leu +0.002% MMS plates and left to grow at 30 °C for three days.
399
400 **Image Acquisition and Analysis**
401 Prior to imaging, cells were washed twice in imaging media SC supplemented with
402 2% galactose or 2% raffinose and mounted on a glass depression slide coated with
403 agarose supplemented with all amino acids. GFP and RFP signals were visualized
404 with Zeiss AxioObserver spinning disk microscope, 63x objective set to acquire 10 z-
405 stack images spaced at 0.4 µm. Z-stacks were imported into Fiji and max-projected
406 to acquire a single image sum of all slices. Foci were counted by adjusting the image
407 color threshold to the average nuclear signal intensity for a given image and
408 counting spherical regions that gave pixel intensity above the threshold. For GFP
409 and RFP colocalization analysis, max projected z-stacks were merged in Fiji and
410 analyzed for overlapping foci. Rad51-GFP nuclear intensities were quantified by
411 measuring the integrated intensities of concentric nuclear circles from max
412 projecting z-stack images and subtracting from this value the average background
413 fluorescent intensities. Ddc2-GFP spot intensities were determined in a similar
414 fashion.
415
416 **Chromatin Immunoprecipitation**
417 Chromatin immunoprecipitation (ChIP) was carried out as described in (58). In
418 brief, cells were harvested from log-phase population. 45 ml of culture were fixed
419 and crosslinked with 1% formaldehyde for 10 minutes after which 2.5 ml of 2.5 M
420 glycine was added for 5 minutes to quench the reaction. Cells were pelleted and
421 washed 3 times with 4°C TBS. Cell wall was disrupted by 1 h bead beating in lysis
422 buffer, after which cells sonicated for 2 minutes. Debris was then pelleted and
423 discarded, and equal volume of lysate was immunoprecipitated using α-ScRad51
424 antibody for 1 hour in 4°C, followed by addition of protein-A agarose beads for 1 h
425 at 4°C. The immunoprecipitate was then salt washed 5 times, and crosslinking was

426 reversed at 65°C overnight followed by proteinase-K addition for 2 h. Protein and
427 nucleic acids where separated by phenol extraction. Chromatin association with
428 Rad51 was assessed by qPCR. More detailed protocols and recipes are available
429 upon request. α-ScRad51 antibodies were a generous gift of A. Shinohara
430 (University of Osaka, Osaka, Japan) and from Douglas Bishop (University of Chicago,
431 Chicago, Il).
432
433 **DSB Repair Analysis by qPCR**
434 Monitoring repair kinetics by qPCR was performed as described previously (59).
435 Single colonies were inoculated in 5ml of -leu dropout media with 2% dextrose and
436 grown overnight at 30C. Overnight cultures were then diluted into 600ml of YPLac
437 and grown into log phase. DSBs were induced by adding 20% galactose to a final
438 concentration of 2%. To track the dynamics of DSB repair 50ml aliquots of each
439 culture was collected every hour over 9 h. DNA was isolated using a MasterPure™
440 Yeast DNA Purification Kit (Epicentre cat. MPY80200). The repair product *MAT*a-inc
441 was amplified using primers MATp13 and MATYp4 with a SYBR Green Master Mix
442 using a Qiagen Rotor-Gene Q real-time PCR machine. To quantify the relative
443 amount of *MAT*a-inc in each sample, Slx4p was used as a reference gene and was
444 amplified using primers NS047-Slx4p7 and Slx4p1. Primer sequences are shown in
445 Table S2.
446
447 **References:**
448 1. Lee JY, Terakawa T, Qi Z, Steinfeld JB, Redding S, Kwon Y, et al. DNA
449 RECOMBINATION. Base triplet stepping by the Rad51/RecA family of recombinases.
450 Science. 2015;349(6251):977-81.
451 2. Bell JC, Kowalczykowski SC. RecA: Regulation and Mechanism of a Molecular
452 Search Engine. Trends in biochemical sciences. 2016;41(6):491-507.
453 3. San Filippo J, Sung P, Klein H. Mechanism of eukaryotic homologous
454 recombination. Annual review of biochemistry. 2008;77:229-57.
455 4. Haber JE. A Life Investigating Pathways That Repair Broken Chromosomes.
456 Annual review of genetics. 2016;50:1-28.

457 5. Alani E, Thresher R, Griffith JD, Kolodner RD. Characterization of DNA-
458 binding and strand-exchange stimulation properties of y-RPA, a yeast single-strand-
459 DNA-binding protein. Journal of molecular biology. 1992;227(1):54-71.
460 6. Raderschall E, Golub EI, Haaf T. Nuclear foci of mammalian recombination
461 proteins are located at single-stranded DNA regions formed after DNA damage. Proc
462 Natl Acad Sci U S A. 1999;96(5):1921-6.
463 7. Sung P. Yeast Rad55 and Rad57 proteins form a heterodimer that functions
464 with replication protein A to promote DNA strand exchange by Rad51 recombinase.
465 Genes Dev. 1997;11(9):1111-21.
466 8. Liu J, Renault L, Veaute X, Fabre F, Stahlberg H, Heyer WD. Rad51 paralogues
467 Rad55-Rad57 balance the antirecombinase Srs2 in Rad51 filament formation.
468 Nature. 2011;479(7372):245-8.
469 9. Sugiyama T, Kowalczykowski SC. Rad52 protein associates with replication
470 protein A (RPA)-single-stranded DNA to accelerate Rad51-mediated displacement of
471 RPA and presynaptic complex formation. J Biol Chem. 2002;277(35):31663-72.
472 10. Duan Z, Andronescu M, Schutz K, McIlwain S, Kim YJ, Lee C, et al. A three-
473 dimensional model of the yeast genome. Nature. 2010;465(7296):363-7.
474 11. Lee CS, Wang RW, Chang HH, Capurso D, Segal MR, Haber JE. Chromosome
475 position determines the success of double-strand break repair. Proc Natl Acad Sci U
476 S A. 2016;113(2):E146-54.
477 12. Oza P, Jaspersen SL, Miele A, Dekker J, Peterson CL. Mechanisms that regulate
478 localization of a DNA double-strand break to the nuclear periphery. Genes Dev.
479 2009;23(8):912-27.
480 13. Horigome C, Oma Y, Konishi T, Schmid R, Marcomini I, Hauer MH, et al. SWR1
481 and INO80 chromatin remodelers contribute to DNA double-strand break
482 perinuclear anchorage site choice. Molecular cell. 2014;55(4):626-39.
483 14. Lao JP, Oh SD, Shinohara M, Shinohara A, Hunter N. Rad52 promotes
484 postinvasion steps of meiotic double-strand-break repair. Molecular cell.
485 2008;29(4):517-24.
486 15. Lisby M, Mortensen UH, Rothstein R. Colocalization of multiple DNA double-
487 strand breaks at a single Rad52 repair centre. Nature cell biology. 2003;5(6):572-7.

16. Miyazaki T, Bressan DA, Shinohara M, Haber JE, Shinohara A. In vivo assembly and disassembly of Rad51 and Rad52 complexes during double-strand break repair. The EMBO journal. 2004;23(4):939-49.

17. Da Ines O, Degroote F, Goubely C, Amiard S, Gallego ME, White CI. Meiotic recombination in Arabidopsis is catalysed by DMC1, with RAD51 playing a supporting role. PLoS Genet. 2013;9(9):e1003787.

18. Cloud V, Chan YL, Grubb J, Budke B, Bishop DK. Rad51 is an accessory factor for Dmc1-mediated joint molecule formation during meiosis. Science. 2012;337(6099):1222-5.

19. Tsabar M, Mason JM, Chan YL, Bishop DK, Haber JE. Caffeine inhibits gene conversion by displacing Rad51 from ssDNA. Nucleic acids research. 2015;43(14):6902-18.

20. Kobayashi W, Sekine S, Machida S, Kurumizaka H. Green fluorescent protein fused to the C terminus of RAD51 specifically interferes with secondary DNA binding by the RAD51-ssDNA complex. Genes Genet Syst. 2014;89(4):169-79.

21. Akamatsu Y, Tsutsui Y, Morishita T, Siddique MS, Kurokawa Y, Ikeguchi M, et al. Fission yeast Swi5/Sfr1 and Rhp55/Rhp57 differentially regulate Rhp51-dependent recombination outcomes. The EMBO journal. 2007;26(5):1352-62.

22. Zou L, Elledge SJ. Sensing DNA damage through ATRIP recognition of RPA-ssDNA complexes. Science. 2003;300(5625):1542-8.

23. Dubrana K, van Attikum H, Hediger F, Gasser SM. The processing of double-strand breaks and binding of single-strand-binding proteins RPA and Rad51 modulate the formation of ATR-kinase foci in yeast. Journal of cell science. 2007;120(Pt 23):4209-20.

24. Dotiwala F, Eapen VV, Harrison JC, Arbel-Eden A, Ranade V, Yoshida S, et al. DNA damage checkpoint triggers autophagy to regulate the initiation of anaphase. Proc Natl Acad Sci U S A. 2013;110(1):E41-9.

25. Lee SE, Moore JK, Holmes A, Umezu K, Kolodner RD, Haber JE. Saccharomyces Ku70, mre11/rad50 and RPA proteins regulate adaptation to G2/M arrest after DNA damage. Cell. 1998;94(3):399-409.

518 26. Shinohara A, Ogawa H, Ogawa T. Rad51 protein involved in repair and
519 recombination in S. cerevisiae is a RecA-like protein. Cell. 1992;69(3):457-70.
520 27. Basile G, Aker M, Mortimer RK. Nucleotide sequence and transcriptional
521 regulation of the yeast recombinational repair gene RAD51. Molecular and cellular
522 biology. 1992;12(7):3235-46.
523 28. Sugawara N, Wang X, Haber JE. In vivo roles of Rad52, Rad54, and Rad55
524 proteins in Rad51-mediated recombination. Molecular cell. 2003;12(1):209-19.
525 29. Sandell LL, Zakian VA. Loss of a yeast telomere: arrest, recovery, and
526 chromosome loss. Cell. 1993;75(4):729-39.
527 30. Toczyski DP, Galgoczy DJ, Hartwell LH. CDC5 and CKII control adaptation to
528 the yeast DNA damage checkpoint. Cell. 1997;90(6):1097-106.
529 31. Lee SE, Pellicioli A, Vaze MB, Sugawara N, Malkova A, Foiani M, et al. Yeast
530 Rad52 and Rad51 recombination proteins define a second pathway of DNA damage
531 assessment in response to a single double-strand break. Molecular and cellular
532 biology. 2003;23(23):8913-23.
533 32. Kim JA, Haber JE. Chromatin assembly factors Asf1 and CAF-1 have
534 overlapping roles in deactivating the DNA damage checkpoint when DNA repair is
535 complete. Proc Natl Acad Sci U S A. 2009;106(4):1151-6.
536 33. Aboussekhra A, Chanet R, Adjiri A, Fabre F. Semidominant suppressors of
537 Srs2 helicase mutations of Saccharomyces cerevisiae map in the RAD51 gene, whose
538 sequence predicts a protein with similarities to procaryotic RecA proteins.
539 Molecular and cellular biology. 1992;12(7):3224-34.
540 34. Forget AL, Loftus MS, McGrew DA, Bennett BT, Knight KL. The human Rad51
541 K133A mutant is functional for DNA double-strand break repair in human cells.
542 Biochemistry. 2007;46(11):3566-75.
543 35. Wilson TE, Grawunder U, Lieber MR. Yeast DNA ligase IV mediates non-
544 homologous DNA end joining. Nature. 1997;388(6641):495-8.
545 36. Teo SH, Jackson SP. Identification of Saccharomyces cerevisiae DNA ligase IV:
546 involvement in DNA double-strand break repair. The EMBO journal.
547 1997;16(15):4788-95.

548 37. Schar P, Herrmann G, Daly G, Lindahl T. A newly identified DNA ligase of
549 Saccharomyces cerevisiae involved in RAD52-independent repair of DNA double-
550 strand breaks. Genes Dev. 1997;11(15):1912-24.
551 38. Llorente B, Symington LS. The Mre11 nuclease is not required for 5' to 3'
552 resection at multiple HO-induced double-strand breaks. Molecular and cellular
553 biology. 2004;24(21):9682-94.
554 39. Wolner B, van Komen S, Sung P, Peterson CL. Recruitment of the
555 recombinational repair machinery to a DNA double-strand break in yeast. Molecular
556 cell. 2003;12(1):221-32.
557 40. Rouse J, Jackson SP. Interfaces between the detection, signaling, and repair of
558 DNA damage. Science. 2002;297(5581):547-51.
559 41. Ball HL, Ehrhardt MR, Mordes DA, Glick GG, Chazin WJ, Cortez D. Function of
560 a conserved checkpoint recruitment domain in ATRIP proteins. Molecular and
561 cellular biology. 2007;27(9):3367-77.
562 42. Melo JA, Cohen J, Toczyski DP. Two checkpoint complexes are independently
563 recruited to sites of DNA damage in vivo. Genes Dev. 2001;15(21):2809-21.
564 43. Nakada S, Katsuki Y, Imoto I, Yokoyama T, Nagasawa M, Inazawa J, et al. Early
565 G2/M checkpoint failure as a molecular mechanism underlying etoposide-induced
566 chromosomal aberrations. The Journal of clinical investigation. 2006;116(1):80-9.
567 44. Smith MJ, Rothstein R. Poetry in motion: Increased chromosomal mobility
568 after DNA damage. DNA repair. 2017;56:102-8.
569 45. Fabre E, Zimmer C. From dynamic chromatin architecture to DNA damage
570 repair and back. Nucleus. 2017:0.
571 46. Dion V, Gasser SM. Chromatin movement in the maintenance of genome
572 stability. Cell. 2013;152(6):1355-64.
573 47. Strecker J, Gupta GD, Zhang W, Bashkurov M, Landry MC, Pelletier L, et al.
574 DNA damage signalling targets the kinetochore to promote chromatin mobility.
575 Nature cell biology. 2016;18(3):281-90.
576 48. Lawrimore J, Barry TM, Barry RM, York AC, Friedman B, Cook DM, et al.
577 Microtubule dynamics drive enhanced chromatin motion and mobilize telomeres in
578 response to DNA damage. Molecular biology of the cell. 2017;28(12):1701-11.

579 49. Villoria MT, Ramos F, Duenas E, Faull P, Cutillas PR, Clemente-Blanco A.
580 Stabilization of the metaphase spindle by Cdc14 is required for recombinational
581 DNA repair. The EMBO journal. 2017;36(1):79-101.
582 50. Plate I, Hallwyl SC, Shi I, Krejci L, Muller C, Albertsen L, et al. Interaction with
583 RPA is necessary for Rad52 repair center formation and for its mediator activity. J
584 Biol Chem. 2008;283(43):29077-85.
585 51. Anand R, Beach A, Li K, Haber J. Rad51-mediated double-strand break repair
586 and mismatch correction of divergent substrates. Nature. 2017;544(7650):377-80.
587 52. Graham TG, Walter JC, Loparo JJ. Two-Stage Synapsis of DNA Ends during
588 Non-homologous End Joining. Molecular cell. 2016;61(6):850-8.
589 53. Lobachev K, Vitriol E, Stemple J, Resnick MA, Bloom K. Chromosome
590 fragmentation after induction of a double-strand break is an active process
591 prevented by the RMX repair complex. Curr Biol. 2004;14(23):2107-12.
592 54. Wach A, Brachat A, Pohlmann R, Philippsen P. New heterologous modules for
593 classical or PCR-based gene disruptions in Saccharomyces cerevisiae. Yeast.
594 1994;10(13):1793-808.
595 55. Gietz RD, Woods RA. Transformation of yeast by lithium acetate/single-
596 stranded carrier DNA/polyethylene glycol method. Methods in enzymology.
597 2002;350:87-96.
598 56. Longtine MS, McKenzie A, 3rd, Demarini DJ, Shah NG, Wach A, Brachat A, et
599 al. Additional modules for versatile and economical PCR-based gene deletion and
600 modification in Saccharomyces cerevisiae. Yeast. 1998;14(10):953-61.
601 57. Hanway D, Chin JK, Xia G, Oshiro G, Winzeler EA, Romesberg FE. Previously
602 uncharacterized genes in the UV- and MMS-induced DNA damage response in yeast.
603 Proc Natl Acad Sci U S A. 2002;99(16):10605-10.
604 58. Tsabar M, Eapen VV, Mason JM, Memisoglu G, Waterman DP, Long MJ, et al.
605 Caffeine impairs resection during DNA break repair by reducing the levels of
606 nucleases Sae2 and Dna2. Nucleic acids research. 2015;43(14):6889-901.
607 59. Sugawara N, Haber JE. Monitoring DNA recombination initiated by HO
608 endonuclease. Methods in molecular biology. 2012;920:349-70.

60. Thomas BJ, Rothstein R. Elevated recombination rates in transcriptionally active DNA. Cell. 1989;56(4):619-30.

Figure Captions:

Fig 1. Rad51-GFP forms a DSB-dependent focus a) Representative images of strain DW58 expressing endogenous Rad51-GFP 6 h after HO induction. Magnification of white boxed nucleus shown to the right. Scale bar = 5 μm. **b)** Representative images of strain DW88 (*rad52*Δ) prepared as in (a). **c)** Representative images of strain DW94 (no HO cut site) prepared as in (a). **d)** Quantification of the number of cells displaying Rad51-GFP foci in strain DW58, DW88, and DW94 at the indicated time. **e)** Background-subtracted fluorescence intensities of nuclei in strains DW58 (WT), DW88 (*rad52*Δ), and DW94 (WT, no HO cut site) 6 h after HO induction as described in (a). Box plots display the median (black bar), mean (+), 25th and 75th percentiles (box ranges), 5th and 95th percentiles (whiskers), and outliers (dots). **f)** Representative image from strain DW89 expressing endogenous Rad51-GFP and Rad52-RFP from its endogenous promoter on a low copy plasmid 3 h after HO induction prepared as in (a) **g)** Quantification of Rad51 ChIP signal at the indicated time after induction of HO. Error bars represent the SD of three biological replicates of >150 cells per experiment.

Fig 2. Rad51-GFP is not dominant negative a) Quantification of the percentage of cells that adapt after 24 h after HO induction in the indicated strain. **b)** Quantification of the percent of viable cells following HO induction and repair through ectopic gene conversion in the indicated derivative of YJK17. Student's t test **** $p \leq 0.0001$.**c)** Quantification of the percentage of cells displaying a focus in the indicated derivative of YJK17 at the indicated time. **d)** qPCR analysis of the timing of DSB repair by gene conversion in the indicated derivatives of YJK17. **e)** Spot dilution assay without and with 0.002% MMS. Error bars represent the SD of three biological replicates.

639

640 **Fig 3. Rad51-GFP is competent in meiosis a)** Percent sporulated cells as
641 determined by light microscopy in the indicated strain. **b)** Quantification of spore
642 viability after tetrad dissection of sporulated cells. Error bars are representative of
643 three biological replicates.

644

645 **Fig 4. Rad51-GFP forms multiple foci in response to multiple DSBs a)**
646 Representative images from strain DW106 expressing endogenous Rad51-GFP and
647 Rad52-RFP from its endogenous promoter 3 h after HO induction. Images prepared
648 as in Figure 1A **b)** Quantification of Rad51-GFP and Rad52-RFP foci in DW106 3 h
649 after induction of HO **c)** Representative images from strain DW280 (6 HO cute sites)
650 expressing endogenous Rad51-GFP 3 h after HO induction prepared as in (a) **d)**
651 Quantification of foci per cell in DW280 as described in (c). Error bars represent the
652 SD of three biological replicates of >150 cells per experiment.

653

654 **Fig 5. Analysis of Ddc2-GFP focus dynamics after 3 DSBs a)** Representative
655 images of 1, 2, or 3 foci in strain VE290 expressing endogenous Ddc2-GFP 3 h after
656 HO induction. *n* = total number of cells displaying the indicated number of foci from
657 three biological replicates. Images prepared as in Figure 1A. **b)** Quantification of
658 Ddc2-GFP foci in strain VE290 (WT) and DW546 (*rad52*Δ) 3 h after HO induction.
659 Error bars represent the SD of three biological replicates totaling 856 (WT) and 592
660 (*rad52*Δ) cells. **c)** Background-subtracted fluorescence intensities of individual foci
661 in strains VE290 (WT) and DW546 (*rad52*Δ) 3 h after HO induction as described in
662 B. Box plots prepared as in Figure 1E. **d)** Time lapse images of Ddc2-GFP in strain
663 VE290 suffering 3 DSBs 3 h after HO induction. Time after first image displayed in
664 seconds below.

665

666 **Fig 6. Microtubule dependent Ddc2 foci dynamics a)** Strain DW547 expressing
667 Ddc2-GFP and Mps3-mCherry 3 h after HO induction. Images prepared as in Figure
668 1A. **b)** Similar to (a) with the addition of 15 µg/ml nocodazole after 2 h of HO
669 induction. c) Quantification of Ddc2-GFP foci from cells in (b). Error bars represent

the SD of three biological replicates of >150 cells per experiment. Student's t test: *** $p \leq 0.001$, ** $p \leq 0.01$.

Table S1. Strains used in this study

Strain	Genotype	Parent Strain	Reference	Figures
JKM179	hoΔ hmlΔ::ADE1 MATα hmrΔ::ADE1 ade1-100 leu2-3,112 lys5 trp1::hisG ura3-52 ade3::GAL10::HO		(25)	2A
VE290	hoΔ hmlΔ::ADE1 MATα hmrΔ::ADE1 ade1-100 leu2-3,112 lys5 trp1::hisG ura3-52 ade3::GAL10::HO Chr6: 97749 nt::HPH:HOcs Chr2: 252kb::HOcs-URA3 ddc2-GFP::TRP1	YCSL004	This study	5A, 5B, 5C
DW52	*MATα hoΔ hmlΔ::ADE1 hmrΔ::ADE1 arg5,6Δ::HPH::MAT**a**-inc ade1-100 leu2,3-112 lys5 trp::hisG ura3-52 ade3::GAL::HO rad51-GGSGGS-GFP::TRP1*	YJK17	This study	2B
DW58	hoΔ hmlΔ::ADE1 MATα hmrΔ::ADE1 ade1-100 leu2-3,112 lys5 trp1::hisG ura3-52 ade3::GAL10::HO *rad51-GGSGGS-GFP::TRP1*	JKM179	This study	1A, 1B, 1D, 1G, 2A
DW65	hoΔ hmlΔ::ADE1 MATα hmrΔ::ADE1 ade1-100 leu2-3,112 lys5 trp1::hisG ura3-52 ade3::GAL10::HO rad51::HPH	JKM179	This study	2A
DW88	hoΔ hmlΔ::ADE1 MATα hmrΔ::ADE1 ade1-100 leu2-3,112 lys5 trp1::hisG ura3-52 ade3::GAL10::HO *rad51-GGSGGS-GFP::TRP1 rad52::KAN*	JKM179	This study	1B, 1D, 1E
DW89	hoΔ hmlΔ::ADE1 MATα hmrΔ::ADE1 ade1-100 leu2-3,112 lys5 trp1::hisG ura3-52 ade3::GAL10::HO *rad51-GGSGGS-GFP::TRP1 +pRad52-RFP (LEU2)*	JKM179	This study	1F
DW94	hoΔ hmlΔ::ADE1 MATα hmrΔ::ADE1 ade1-100 leu2-3,112 lys5 trp1::hisG ura3-52 ade3::GAL10::HO *rad51-GGSGGS-GFP::TRP1 -HOcs*	JKM179	This study	1C, 1D
DW106	hoΔ hmlΔ::ADE1 MATα hmrΔ::ADE1 ade1-100 leu2-3,112 lys5 trp1::hisG ura3-52 ade3::GAL10::HO Chr6: 97749 nt::HPH:HOcs Chr2: 252kb::HOcs-URA3 rad51-GGSGGS-GFP::TRP1 +pRad52-RFP(LEU2)	YCSL004	This study	4A, 4B
DW280	Mata *leu2-3,112 trp1-1 ura3-1 can1-100 ade2-1 his3-11,15 RAD5 6 Ty1-HOcs-HIS3 rad51-GGSGGS-GFP::TRP1 +pGAL-HO(TRP1)*	LSY1228	This study	4C, 4D
DW539	*MATα hoΔ hmlΔ::ADE1 hmrΔ::ADE1 arg5,6Δ::HPH::MAT**a**-inc ade1-100 leu2,3-112 lys5 trp::hisG ura3-52 ade3::GAL::HO rad51-GGSGGS-GFP::TRP1 +pRS315(LEU2)*	YJK17	This study	2B, 2C, 2D
DW540	*MATα hoΔ hmlΔ::ADE1 hmrΔ::ADE1*	YJK17	This study	2B. 2C, 2D

	*arg5,6Δ::HPH::MAT**a**-inc ade1-100 leu2,3-112 lys5 trp::hisG ura3-52 ade3::GAL::HO rad51-GGSGGS-GFP::TRP1 +pRad51(LEU2)*			
DW546	hoΔ hmlΔ::ADE1 MATα hmrΔ::ADE1 ade1-100 leu2-3,112 lys5 trp1::hisG ura3-52 ade3::GAL10::HO *ddc2-GFP::TRP1 rad52::KAN*	YCSL004	This study	5B, 5C
DW558	hoΔ hmlΔ::ADE1 MATα hmrΔ::ADE1 ade1-100 leu2-3,112 lys5 trp1::hisG ura3-52 ade3::GAL10::HO *ddc2-GFP::TRP1 mps3-mCherry::KAN*	YCSL004	This study	6A, 6B, 6C
W303-1A	MAT**a** {leu2-3,112 trp1-1 can1-100 ura3-1 ade2-1 his3-11,15		(60)	3A, 3B
W303-1B	MATα {leu2-3,112 trp1-1 can1-100 ura3-1 ade2-1 his3-11,15		(60)	3A, 3B
DW504	MAT**a** {leu2-3,112 trp1-1 can1-100 ura3-1 ade2-1 his3-11,15 rad51-GGSGGS-GFP::TRP1	W303	This study	3A, 3B
DW505	MATα {leu2-3,112 trp1-1 can1-100 ura3-1 ade2-1 his3-11,15 rad51-GGSGGS-GFP::KAN	W303	This study	3A, 3B
DW554	MATα/a {leu2-3,112 trp1-1 can1-100 ura3-1 ade2-1 his3-11,15 rad51-GGSGGS-GFP::KAN/rad51-GGSGGS-GFP::TRP1	W303	This study	3A, 3B
DW123	hoΔ hmlΔ::ADE1 MATα hmrΔ::ADE1 ade1-100 leu2-3,112 lys5 trp1::hisG ura3-52 ade3::GAL10::HO Chr6: 97749 nt::HPH:HOcs Chr2: 252kb::HOcs-URA3 rad51-GGSGGS-GFP::TRP1 lig4::NAT	YCSL004	This study	S2B

674

675 **Table S2. Primers used in this study**

Primer Name	Sequence	Use
VE085 Ddc2-GFP For	ATCTAACCACACTAGAGGAGGCCGATTCATTATATATCTCAATGGGACTG*GGTGGTTCCGGTGGTTCC*CGGATCCCCGGGTTAATTAA	C terminal GFP tagging of Ddc2 (forward)
VE086 Ddc2-GFP Rev	ATTACAAGGTTTCTATAAAGCGTTGACATTTTCCCCTTTTGATTGTTGCCGAATTCGAGCTCGTTTAAAC	C terminal GFP tagging of Ddc2 (reverse)
DW060 Rad51-GFP 2F	CTATGAAGATGGTGTTGGTGACCCCAGAGAAGAAGACGAG*GGTGGTTCCGGTGGTTCC*CGGATCCCCGGGTTAATTAA	C terminal GFP tagging of Rad51 (forward)
DW063 Rad51-GFP 1R	GAAAGTAAACCTGTGTAAATAAATAGAGACAAGAGACCAAATACGAATTCGAGCTCGTTTAAAC	C terminal GFP tagging of Rad51 (reverse)
RAD51HPH1	ATGTCTCAAGTTCAAGAACAACATATATCAGAGTCACAGCTTCAGTACGGGCATAGGCCACTAGTGGATCTG	Genomic deletion of RAD51 with HPH (forward)
RAD51HPH1	CTACTCGTCTTCTTCTCTGGGGTCACCAACACCATCTTCATAGATCGCGATTTCAGCTGAAGCTTCGTACGC	Genomic deletion of RAD51 with HPH (reverse)
DW091 Rad52 1F	GGAGGTTGCCAAGAACTGCTGAAGGTTCTGGTGGCTTTGGTGTGTTGTTGATGCGTACGCTGCAGGTCGAC	Genomic deletion of RAD52 with KAN (forward)
DW092 Rad52 1R	AGTAATAAATAATGATGCAAATTTTTTATTTGTTTCGGCCAGGAAGCGTTTCAATCGATGAATTCGAGCTCG	Genomic deletion of RAD52 with KAN (reverse)

DW493 mps3GFP 1F	CATCCCGCTTCTAACGTCCCATCATTTGGCCAAGATGAGC TAGATCAACGGATCCCCGGGTTAATTAA	C terminally tag mCherry tag Mps3 (forward)
DW494 mps3GFP 1R	CGATTTTCTGGGGGCCAGGGGGTTAGAACGTTTAATTTTT TATTGTCGTGAATTCGAGCTCGTTTAAAC	C terminally tag mCherry tag Mps3 (reverse)
DW265 Rad51 3F	CCGTAGTTTCCATATACTAGTAGTTGAG	Confirm deletion / GFP tagging (forward)
DW266 Rad51 3R	AGATAAAAATGTACGGAACGCAACC	Confirm deletion / GFP tagging (reverse)
ddc2-400 FP	CGTATTGTGTGGCACCGATGTTAAGCAC	Confirm GFP tagging (forward)
ddc2+400 RP	CTCACACCTTGTGTAACAGATGTGGTCG	Confirm GFP tagging (reverse)
DW093 Rad52 2F	CCTGTAATGTCCTTTCGTCTTC	Confirm deletion (forward)
DW094 Rad52 2R	CGACACATGGAGGAAAGAAAA	Confirm deletion (reverse)
MATp13	GTTAAGATAAGAACAAACAAgGATGCT	Monitor repair by qPCR Chr3 201210-201183
MATYp4	GATCTAAATAAATTCGTTTTCAATGATTAAAATAG	Monitor repair by qPCR Chr3 294342-294342
CSL177-Yalpha p1	CTCACAGTTTGGCTCCGGTG	Chr3 200750-200769
NS047-Slx4p7	ACCACTAAGTGACAAAGAACTACG	Chr12 413147-413124 Crick R-L
Slx4p1	GATATGGACCTCTGTCCTTCCT	Chr12 412956-412977 Watson L->R

Supplementary Figure Legends:

Figure S1: Rad51-GFP localization._**a**) Representative full field image of strain DW58 expressing endogenous Rad51-GFP 6 h after HO induction. **b**) Representative full field image of strain DW88 (*rad52*Δ) expressing Rad51-GFP 6 h after HO induction. **c)** Representative images of strain DW94 (no HO cut site) expressing Rad51-GFP 6 h after HO induction. **d**) Representative full field image from strain DW89 expressing endogenous Rad51-GFP and Rad52-RFP from its endogenous promoter on a low copy plasmid 3 h after HO induction. Maximum projection of 12 z-stack images every 0.4 µm. Scale bar = 5 um

Figure S2: Rad51-GFP localization in multi-break strains a)_Representative full field images of strain DW106 expressing Rad51-GFP and Rad52-RFP 3 h after HO induction. b) Quantification of Rad51-GFP foci in strain DW123 (*lig4*Δ) **c**)

691 Representative full field images of strain DW280 expressing Rad51-GFP 3 h after HO
692 induction. Maximum projection of 12 z-stack images every 0.4 µm. Scale bar = 5 um
693
694 **Figure S3: Ddc2-GFP localization in multi-break strains a)** Representative full
695 field image of strain VE290 expressing Ddc2-GFP 3 h after HO induction. **b**)
696 Representative full field image of strain DW546 (*rad52*Δ) expressing Ddc2-GFP 3 h
697 after HO induction. Maximum projection of 12 z-stack images every 0.4 um. Scale
698 bar = 5 µm
699
700 **Movie S4 – S6** Ddc2-GFP in 3 DSB strain DW546 (*rad52*Δ) 3 h after HO induction.
701 Scale bar = 5 µm.
702
703 **Movie S7 – S17** Ddc2-GFP in 3 DSB strain VE290 3 h after HO induction. Scale bar =
704 5 µm.

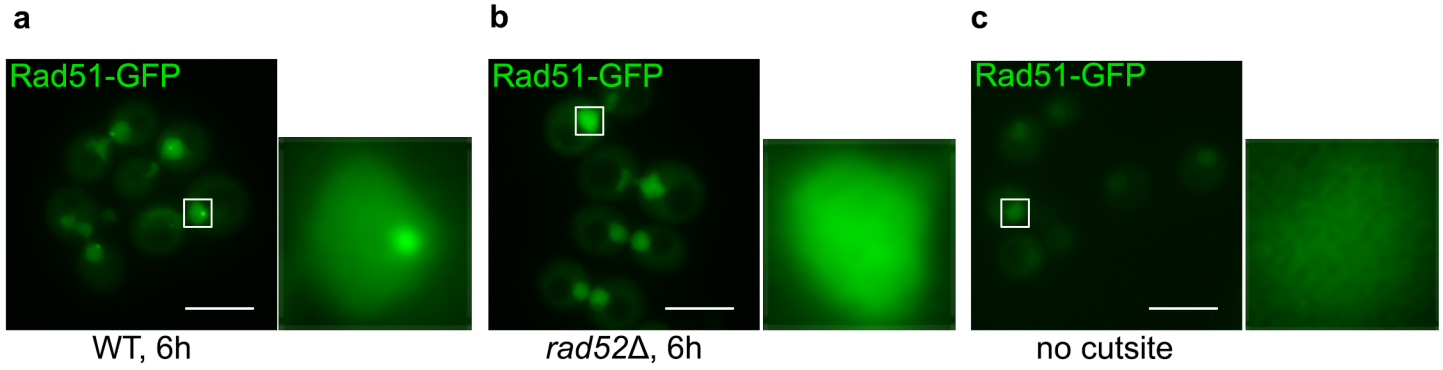

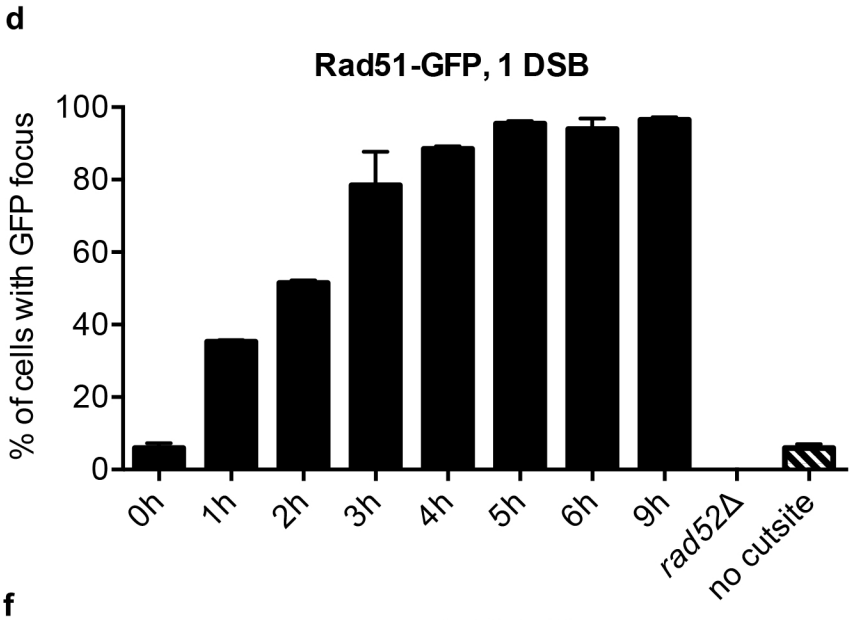

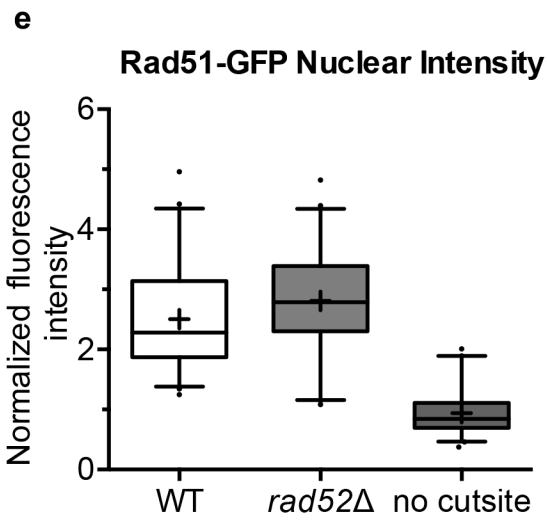

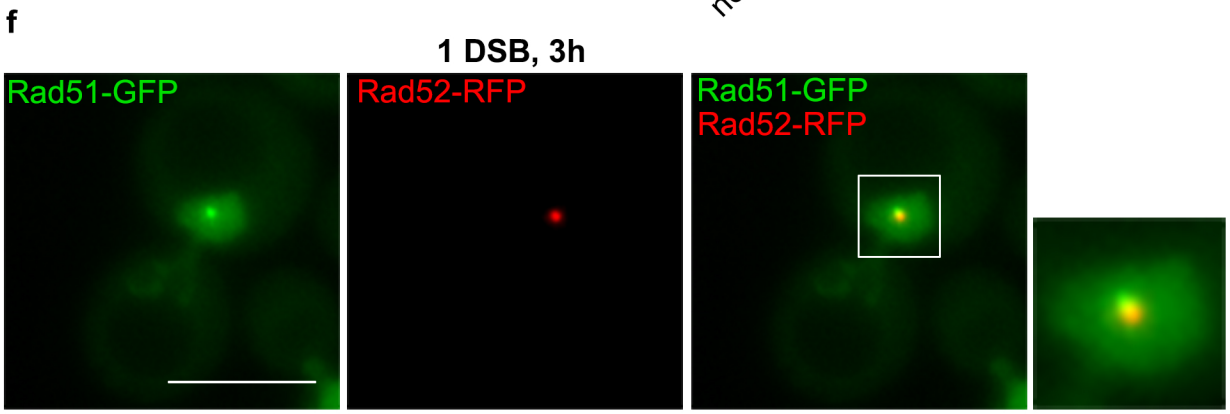

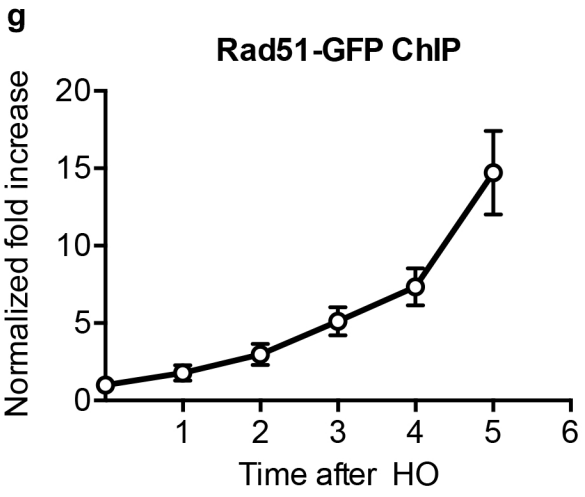

Figure 1

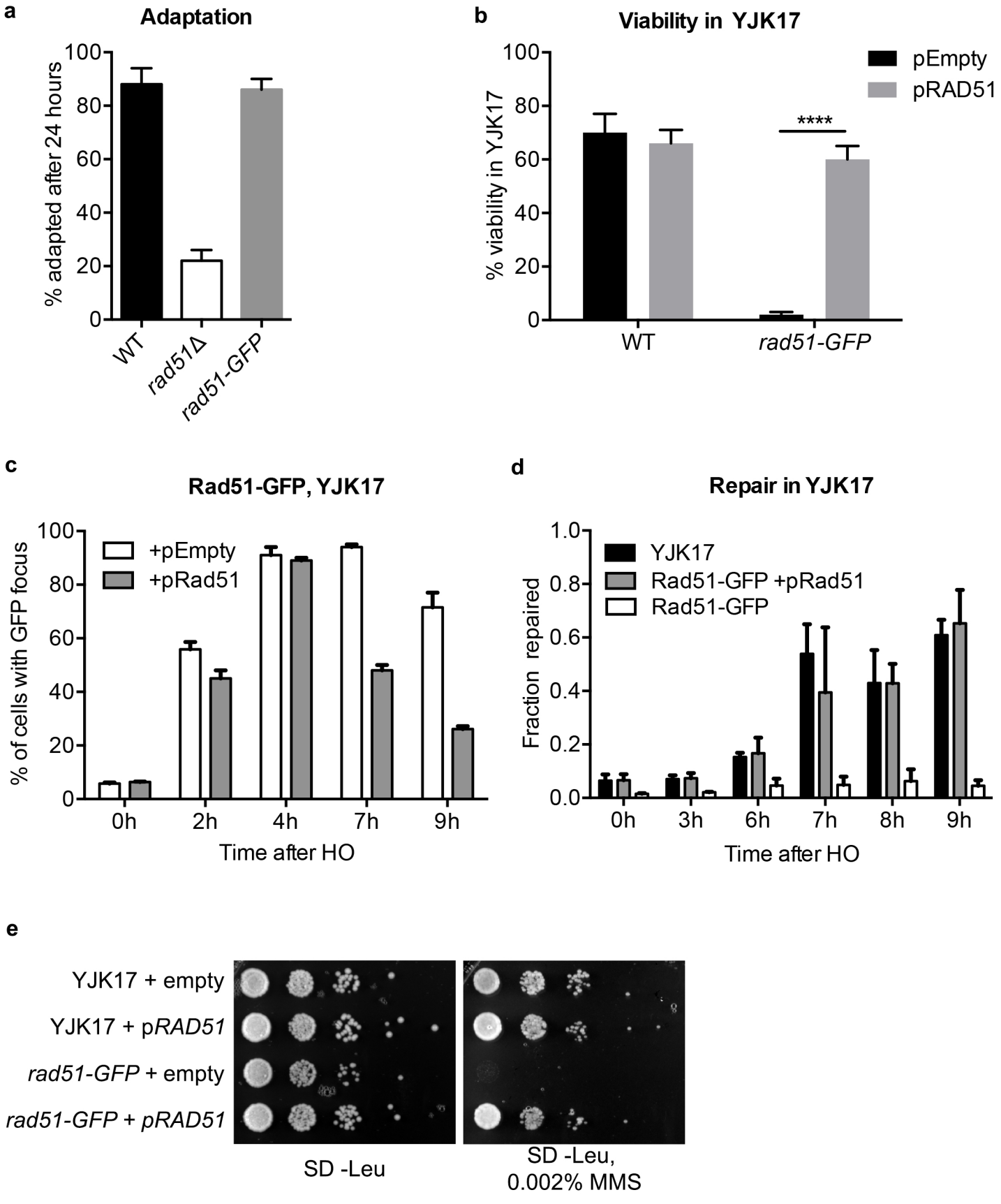

Figure 2

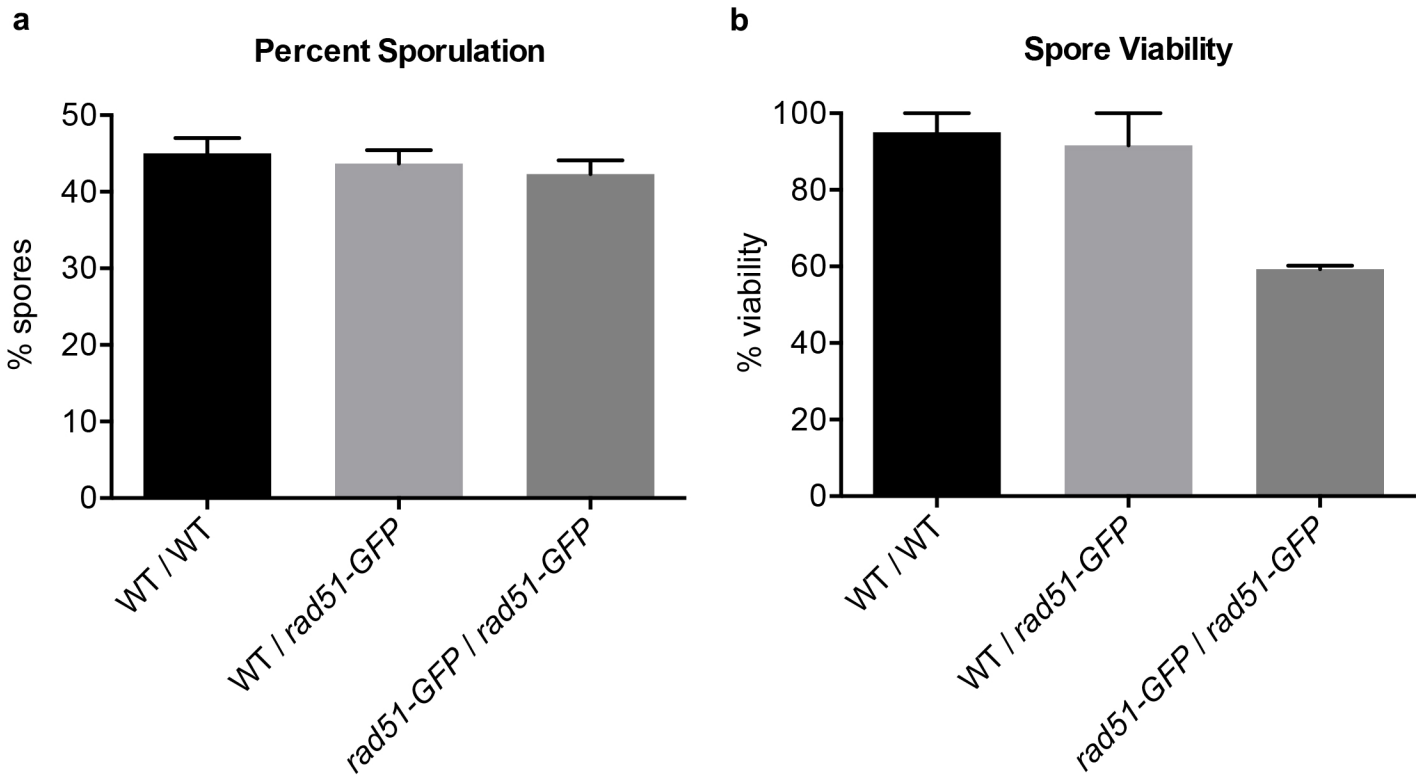

Figure 3

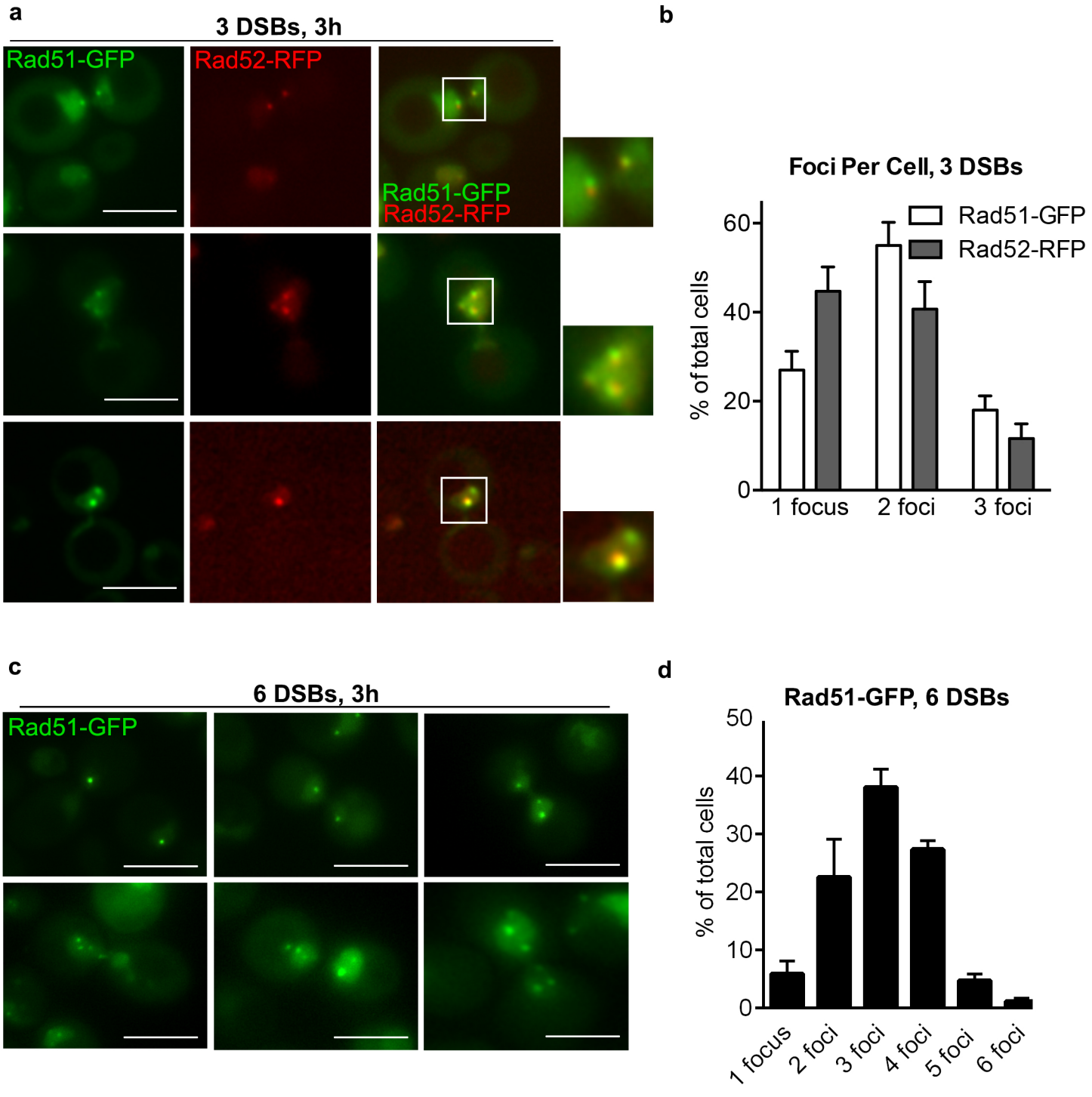

Figure 4

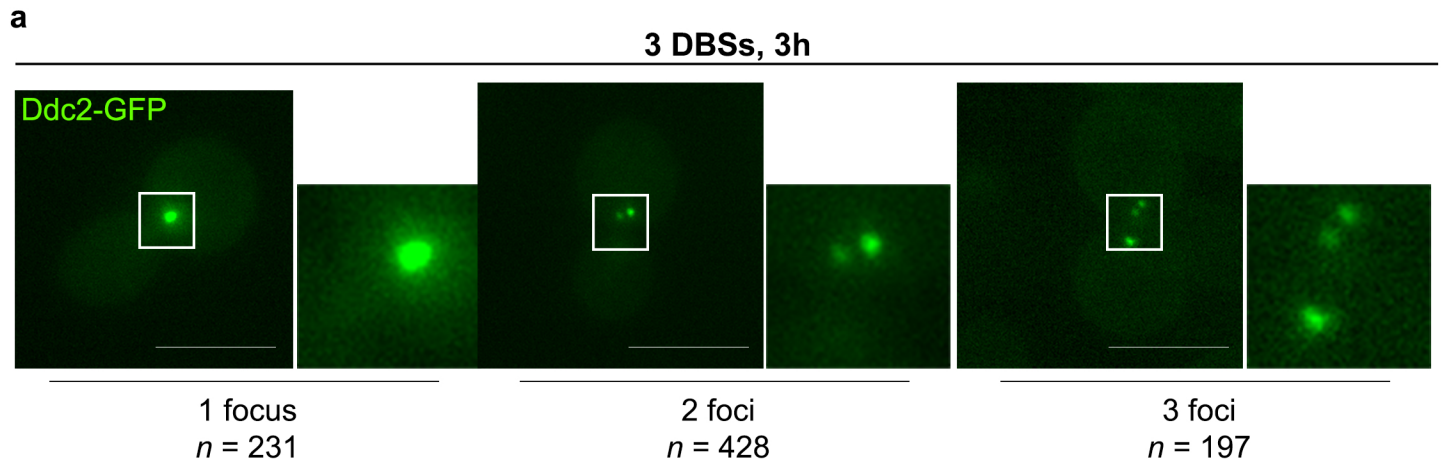

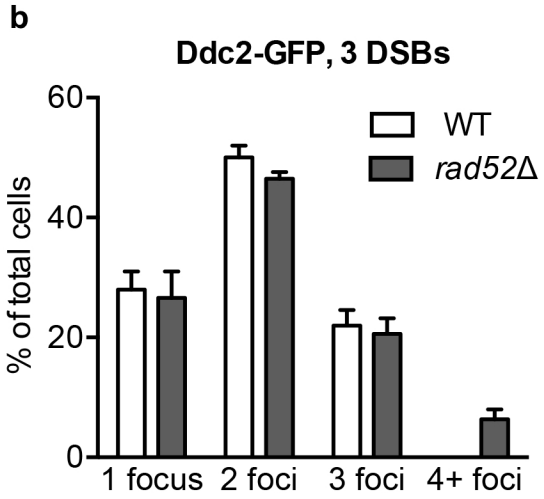

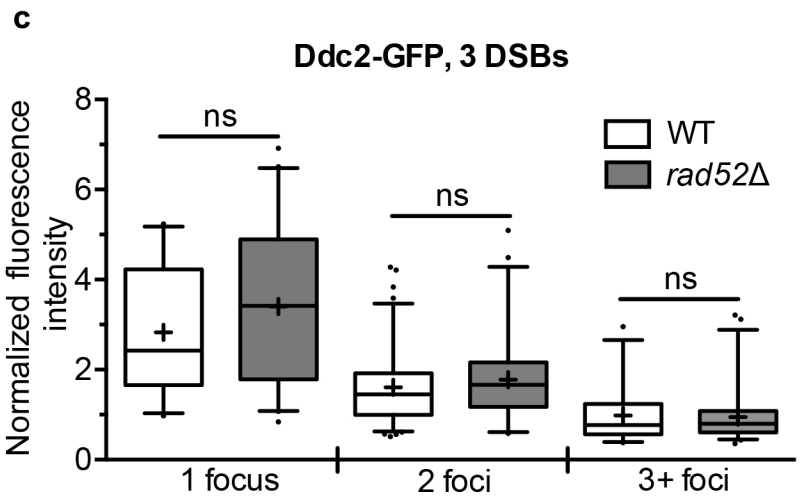

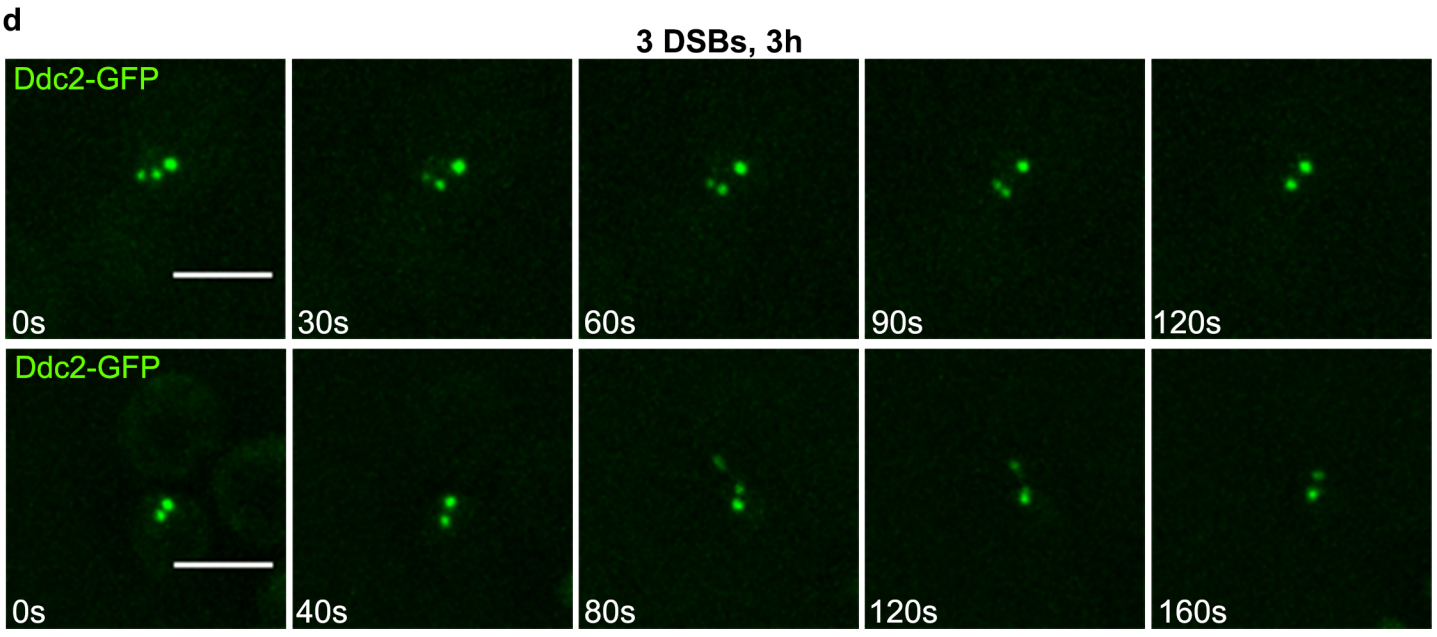

Figure 5

a

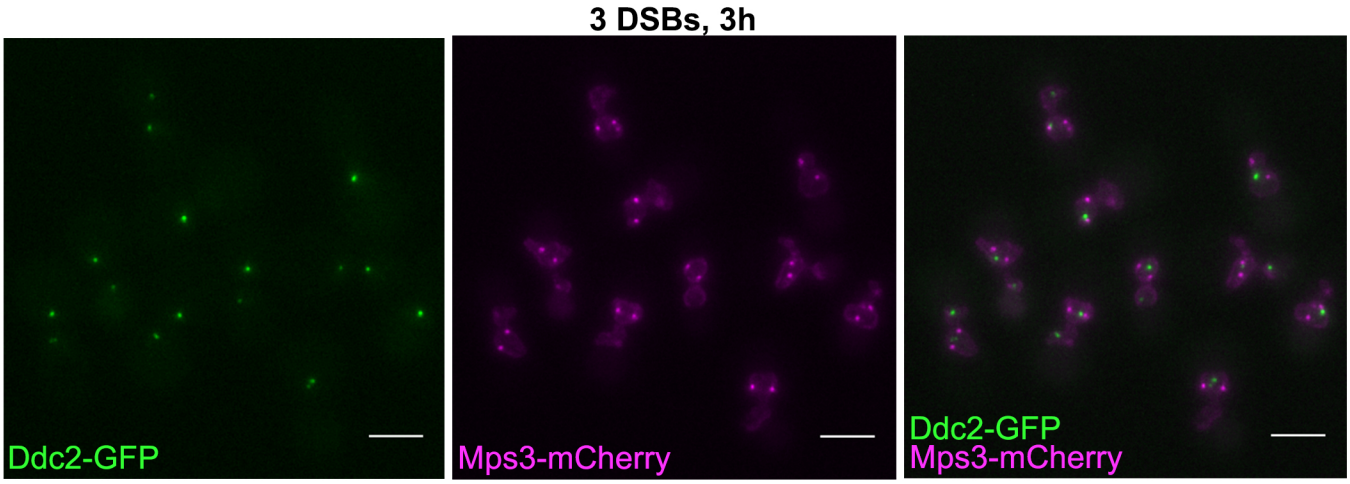

b

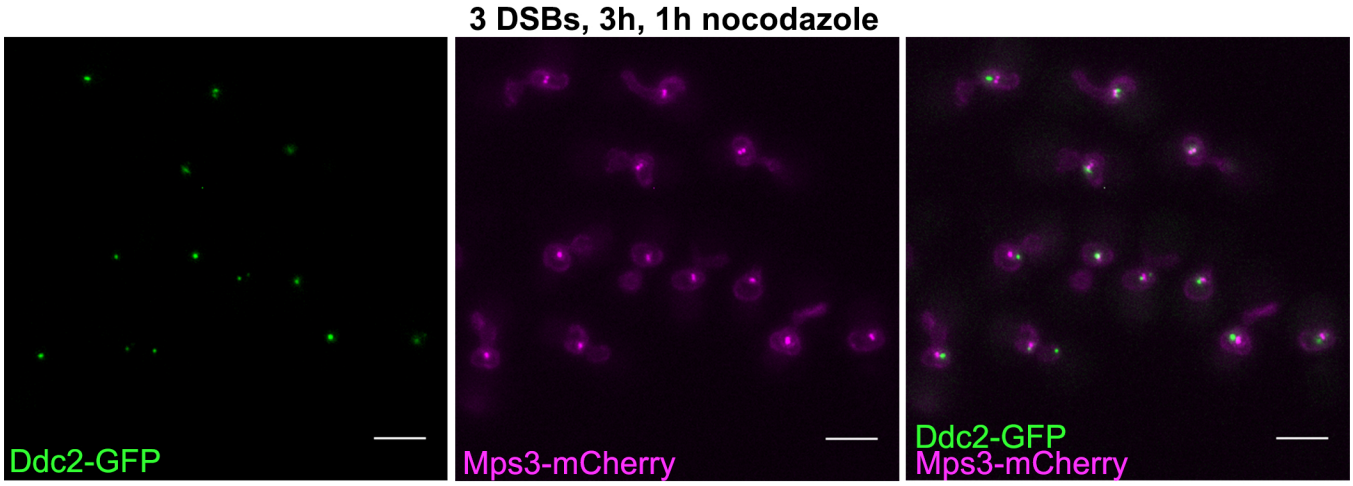

c

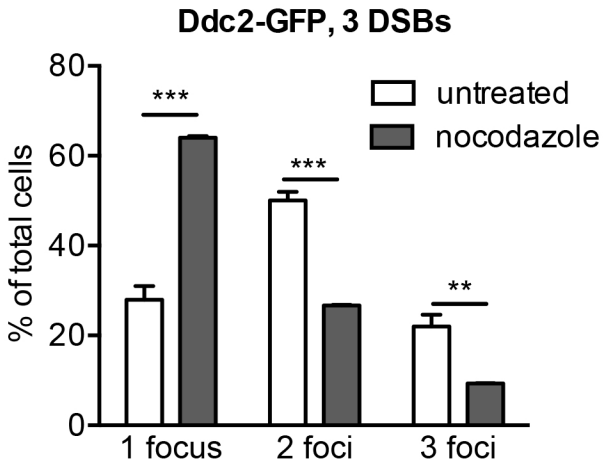

Figure 6